Monoanionic Phosphorus-Supported Air Stable Cu(I)$_8$, Ag(I)$_7$, and Ag(I)$_5$ Nanoclusters Exhibiting TADF: A Novel Photocatalyst for Stereoselective Carbene Transfer Reactions

Ekta Nag, Asutosh Patra, Maria Francis, Usharani Patra, and Sudipta Roy*

Applications of structurally well-defined coinage-metal nanoclusters (NCs) as optoelectronic materials and homogeneous catalysts have been restricted due to their inherent lower stability. Herein, the syntheses, structural characterizations, and photoluminescence properties of three novel air-stable coinage-metal(I) NCs-supported by carbene-anchored monoanionic phosphorus (cAAC=P$^-$) with molecular formulae [(Cy-cAACP)$_4$(Cu)$_4$(CuCl)$_4$] (4), [(Cy-cAACP)$_4$(Ag)$_4$(AgOTf)$_3$] (5), and [(Cy-cAACP)$_4$(Ag)$_5$]NTf$_2$ (6) (cAAC = cyclic alkyl(amino) carbene; Tf = CF$_3$SO$_2$) exhibiting thermally activated delayed fluorescence (TADF) are reported. Apart from attractive metallophilic interactions [M—M; M = Cu, Ag], the enhanced kinetic and thermodynamic stability of 4–6 can be attributed to the excellent π-accepting ability of cAAC=P$^-$ surrounding the metallic cores. cAAC=P$^-$ anion is generated either in situ by anion-induced cleavage of P—Sb/B bonds of corresponding stibanyl/boryl phosphaalkenes in the presence of coinage-metal(I)-Cl/OTf/NTf$_2$ salts or by directly introducing alkali-metal phosphinidenide. The TADF properties of 4–6 are established by smaller energy gaps between the lowest singlet excited state and triplet excited state. In solid-state, the delayed fluorescence lifetimes of 4–6 are found to be in the microsecond range with absolute photoluminescence quantum yields up to 20%. The redox-active Cu(I)$_8$ NC 4 is successfully exploited as an efficient photo-catalyst for the selective carbene transfer reaction at ambient conditions, affording cyclopropanated indoles/styrenes with excellent yields and diastereoselectivity.

1. Introduction

Luminescent coinage metal nanoclusters (NCs) exhibiting thermally activated delayed fluorescence (TADF) with smaller singlet-triplet energy gap $\Delta E(S_1\text{-}T_1)$, and weaker spin-orbit coupling have recently attracted huge attention not only because of their application in the manufacturing of efficient organic light-emitting diodes (OLEDs),[1,2] but also due to their potential usage in the field of homogeneous catalysis,[3] chemical sensing, and bio-imaging/labeling.[4] The delayed emission takes place from the lowest excited singlet state S_1 to the ground state S_0 via reverse intersystem crossing (RISC) from the triplet excited state T_1 to S_1 upon thermal activation at ambient temperature (**Figure 1**).[5] Through this process, all the generated singlet and triplet excitons can be harvested from the lowest singlet excited state, S_1, and thereby the OLED generated using such materials can have nearly 100% internal quantum efficiency. TADF materials with a larger radiative rate constant at S_1 compared to that of a non-radiative process can have higher emission quantum yields. However, the stability and/or structural rigidity of the NCs at various temperatures play a crucial role to reduce the non-radiative decay, and hence obtaining a better photoluminescence quantum yield (PLQY), Φ_{PL}.

In general, the formation of a well-defined metal NC largely depends on the specific electronic and steric environments exerted by the stabilizing ligands, which in turn significantly controls the molecular properties of such species, e.g., the specific absorption features, photoluminescence, optical activity, polymorphism, etc. In this regard, syntheses of atomically precise Ag, and Cu NCs are more challenging compared to the Au NCs considering the inherently weaker cohesive energy in the former, and the spontaneous tendency toward aerial oxidation in the latter due to the lower standard reduction potential. Therefore, a careful selection of the stabilizing ligand becomes extremely important for the syntheses of such species. The solid–state isolation of so far reported Ag-based NCs mainly relies on various soft and hard ligand systems, viz., alkynyl,[6] thiolates,[7] sulfonate,[8] phosphonate,[9] phosphine,[10] carboxylate,[11] amine,[12] and very recently the cyanurate[13] derivatives. On the other hand, the potential ligand systems identified for the stabilization of Cu-based NCs include thiolates, di-thiocarbamates, sulfides, phosphines, halides, carboxylates, alkynes, and hydrides.[14] However, the major challenge still remains with the stability, and solubility of these NCs to be effectively utilized for generation of

E. Nag, A. Patra, M. Francis, U. Patra, S. Roy
Department of Chemistry
Indian Institute of Science Education and Research (IISER)
517507 Tirupati, India
E-mail: roy.sudipta@iisertirupati.ac.in

The ORCID identification number(s) for the author(s) of this article can be found under https://doi.org/10.1002/adom.202301256
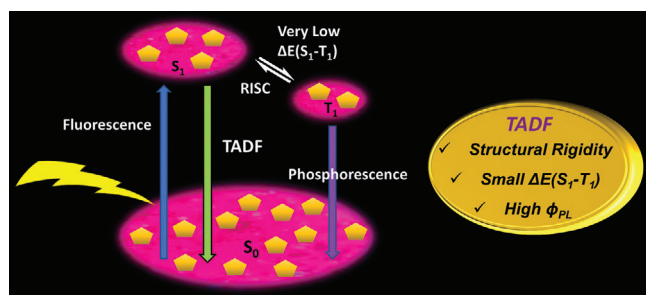
Figure 1. Schematic representation of various electronic transitions including fluorescence, phosphorescence, and thermally activated delayed fluorescence (TADF).
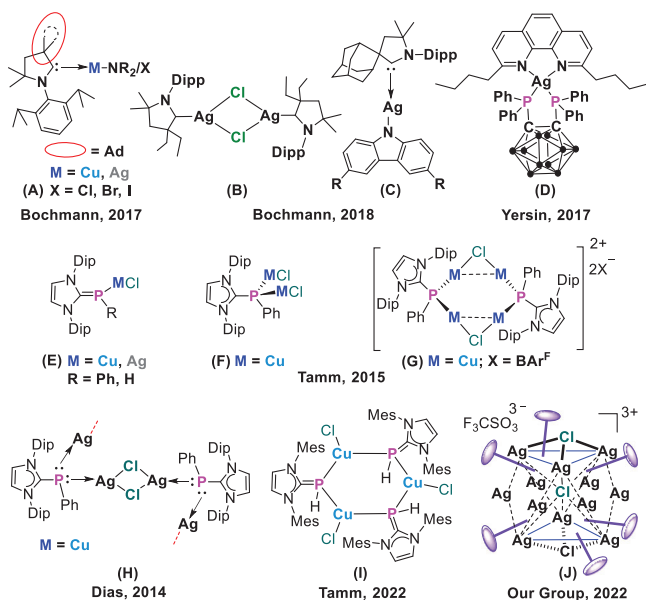

Figure 2. Representative Cu(I), and Ag(I) complexes stabilized by carbenes and carbene-supported phosphinidenes.

OLEDs. Softer ligands, e.g., phosphines bind very weakly to the metal centers, increasing the lability; whereas, the harder ligands, e.g., alkynes, thiolates, etc. bind to the metal centers too specifically in an unalterable fashion, enabling the exchange of metal atoms leading to a decrease of the overall cluster stability. The synthetic main group chemistry community has very often witnessed the superiority of carbenes over other σ-donor ligands; more precisely, with cyclic alkyl(amino) carbenes (cAACs) as ligands addressing various synthetic challenges.[15] With respect to the exciting photoluminescence properties exhibited by the donor base-stabilized metal complexes, cAAC has achieved remarkable success in the past decade.[16] In 2017, Di et al. reported two-coordinate carbene-Cu-X, and carbene-Ag-X (X = Cl, Br, I) complexes, **A** (**Figure 2**) with exciting green emissions having maximum external efficiency of 9.7–26.3%.[16a] The luminescent cAAC-Ag(I)-amide complexes (**C**) exhibiting TADF properties are also noteworthy in this regard (Figure 2).[16]

From our recent experience on isolation of higher nuclearity homo- and/or mixed valence Ag NCs, e.g., **J** (Figure 2)[17]: presuming that the combination of a soft/hard ligand system together might greatly overcome the stability issue of the NCs, we
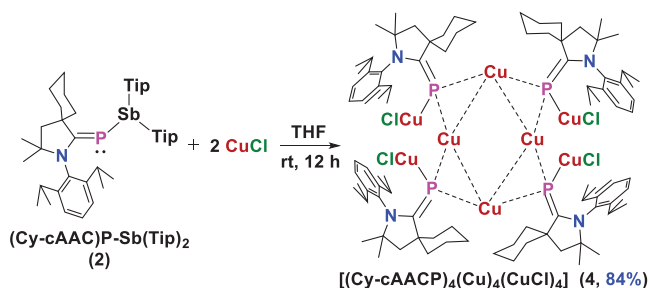
decided to probe the applicability of the cAAC-supported mono-anionic phosphorus, cAAC=P$^-$[17] for the syntheses of structurally well-defined Cu, and Ag NCs with exciting luminescence properties. While carbene being a harder donor (C donor site), and phosphorus (P donor site) being a softer donor, a combination of both can lead to unusual coordination modes, resulting in novel cluster formation with increased structural rigidity, leading to a reduced non-radiative decay rate along with the exciting luminescence features. Considering the ease of in situ generation of the monoanionic phosphorus atom from the easily available alkali metal phosphinidenides (**1**)[18] in pure crystalline form and quantitative yields, we have chosen **1** as the source of the stabilizing ligand for synthesizing novel coinage metal NCs. So far, there are only a very few examples of the coinage metal complexes stabilized by carbene-phosphinidenides, **E**–**I** (Figure 2).[19,20] Moreover, the existence of nano-sized coinage metal clusters of cAAC-supported phosphinidenides is extremely rare.[17]

Utilizing the unique steric and electronic effects of combined cAAC and monoanionic phosphorus, herein, we report on the first syntheses, structural characterization, and detailed photoluminescence studies of three novel air-stable NCs containing Cu$_8$, Ag$_7$, and Ag$_5$ cores with well-defined molecular formulae [(Cy-cAACP)$_4$(Cu)$_4$(CuCl)$_4$] (**4**), [(Cy-cAACP)$_4$(Ag)$_4$(AgOTf)$_3$] (**5**), and [(Cy-cAACP)$_4$(Ag)$_5$]NTf$_2$ (**6**).

2. Results and Discussion

Initially, the dark red crystals of cyclic alkyl(amino) carbene (cAAC)-supported potassium phosphinidenide (cAACPK, **1**)[21] were treated with CuCl in various molar ratios in THF as solvent at room temperature (rt). However, in all the cases the respective ^{1}H NMR spectra of the crude reaction mixtures showed the presence of either cAACPH[22] or cAAC$_2$P$_2$.[23] Failing to utilize cAACPK as the direct source of monoanionic phosphorus, we decided to employ the cAAC-supported stibanyl-phosphaalkene (Cy-cAAC)P—Sb(Tip)$_2$ (**2**) (Cy-cAAC = C(N-2,6-^{i}Pr$_2$C$_6$H$_3$)(C$_6$H$_{10}$)(CMe$_2$)(CH$_2$), Tip = 2,4,6-triisopropylphenyl),[24] which was treated with CuCl in 1:2 molar ratio at rt in THF. The resulting reaction mixture was kept for overnight (12 h) stirring at rt to obtain a clear orange solution. Upon removal of THF under high vacuum, an orange crystalline solid was isolated, which was washed with n-hexane to remove the soluble impurities, and further dissolved in DCM. The orange-red block shaped single crystals of neutral cAAC-phosphinidenide-stabilized Cu(I)$_8$-cluster [[(Cy-cAACP)$_4$(Cu)$_4$(CuCl)$_4$] (**4**) were obtained after 5–7 days from the concentrated DCM solution (1–2 mL) stored at −40 °C in 84% yield (**Scheme 1**).

When stibanyl-phosphaalkene (**2**) was treated with the heavier group 11 halide, viz., AgCl, and AgBr under similar reaction conditions; although the colors of individual reaction mixtures changed from bright yellow to orange, no crystals of the corresponding metal complexes/clusters could be isolated. The ^{31}P NMR spectra of the crude reaction mixtures showed the formation of only Cy-cAACPH.[22] On the other hand, when Cy-cAAC-supported boryl-phosphaalkene (Cy-cAAC)P—B(N^{i}Pr$_2$)$_2$ (**3**)[24] was treated with AgOTf in a 2:1 molar ratio at rt in toluene, a clear yellowish-brown reaction solution was obtained, which was stirred for 12 h at rt, resulting in the formation of a brown color

ADVANCED
SCIENCE NEWS

www.advancedsciencenews.com

ADVANCED
OPTICAL
MATERIALS

www.advopticalmat.de

Scheme 1. Synthesis of carbene-phosphinidenide-stabilized neutral Cu(I)$_8$-nanocluster [(Cy-cAACP)$_4$(Cu)$_4$(CuCl)$_4$] (**4**).
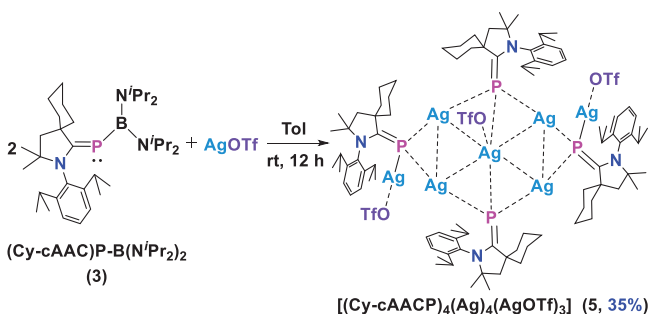
Scheme 2. Synthesis of carbene-phosphinidenide-stabilized neutral Ag(I)$_7$-cluster [(Cy-cAACP)$_4$(Ag)$_4$(AgOTf)$_3$] (**5**).

Scheme 3. Synthesis of carbene-phosphinidene-stabilized mono-cationic Ag(I)$_5$-cluster [(Cy-cAACP)$_4$(Ag)$_5$]NTf$_2$ (**6**).

precipitate. Upon filtration of the reaction mixture through a frit, a brown crystalline residue was obtained, which was washed a couple of times with cold *n*-hexane, and dissolved in DCM. The DCM solution was further concentrated under reduced pressure upto 1–2 mL, and stored at −20 °C to form the block-shaped bright orange color single crystals of Ag(I)$_7$-cluster [(Cy-cAACP)$_4$(Ag)$_4$(AgOTf)$_3$] (**5**) in 35% yield after 10 days (**Scheme 2**). In this context, it is noteworthy to mention that the reaction of **3** with AgOTf in a 1:1 molar ratio at rt in toluene affords two different Ag NCs: the tri-cationic [(Cy-cAACP)$_6$Ag$_{12}$Cl$_3$](OTf)$_3$, and the neutral mixed-valence [(Cy-cAACP)$_6$Ag$_{29}$], which we have reported very recently.[17]

An analogous reaction of boryl-phosphaalkene **3** with AgNTf$_2$ in 2:1, and 1:1 molar ratios at rt in toluene resulted in brownish-red solutions from which no crystals could be isolated even after stirring the reaction mixtures for 12–24 h. The ^{31}P NMR analysis of the reaction mixtures indicated the disappearance of the starting material **3**, and the formation of the corresponding bis-phosphinidene, cAAC$_2$P$_2$.[23] However, when cAACPK (**1**) was treated with AgNTf$_2$ in 2:1 molar ratio at −40°C using toluene as a solvent for 30 min, and further stirred at rt for 12 h, the color of the reaction mixture changed from dark red to greenish-brown. Upon removal of toluene, a yellowish-red crystalline solid was obtained, which was extracted in DCM to give rise to a yellowish-red solution along with the formation of some insoluble black precipitate. The DCM solution was filtered, and concentrated under reduced pressure to obtain orange color block shaped single crystals of Ag(I)$_5$ NC [(Cy-cAACP)$_4$(Ag)$_5$]NTf$_2$ (**6**) from a −40°C freezer in 24% yield (**Scheme 3**).

The crystals/powders of **4–6** were found to be stable under an argon atmosphere for more than a year. Upon exposure to air, the crystals of **4** were found to be stable for 2 days at rt, and then
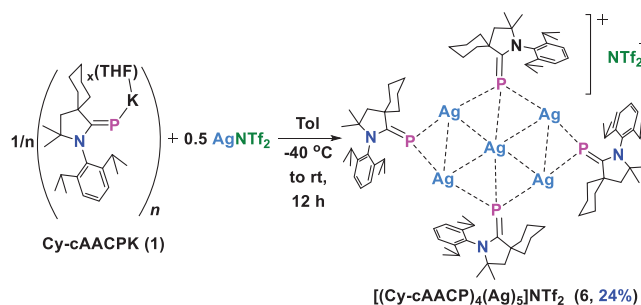
slowly decomposed to a yellow powder. The crystals of **5**, and **6** were found to be stable in air for about a week, which has been concluded from NMR studies. The clusters **4–6** were found to be sparingly soluble in toluene/THF, and highly soluble in DCM. The yellow color DCM solution of **4** was found to be stable in air for an hour, and then slowly turned into a colorless solution with the formation of insoluble black precipitate. However, the DCM solutions of **5**, and **6** were found to be stable in air for a week. Under an inert atmosphere, the DCM solutions of **4–6** were found to be stable at rt for more than six months. The powder of **4**, **5**, and **6** melted to brown liquids at 215–217°C, 175–177°C, and 150–152°C, respectively.

The solution structures for the NCs **4–6** were thoroughly analyzed by NMR, and ESI-MS studies (see Supporting Information). At rt, the ^{31}P NMR spectrum of the DCM-d_2 solution of the Cu(I)$_8$ nanocluster **4** exhibited a very weak singlet at −74.4 ppm, which eventually became intense upon cooling down to 213 K. The ^{31}P spectrum of the DCM-d_2 solutions of the Ag(I)$_7$ nanocluster **5** did not show any signal at rt. However, upon lowering the temperature to 233 K, a triplet was observed at −127.3 ppm ($J_{31P-109Ag}$ = 767.6 Hz), which is downfield shifted when compared to that of the previously reported tri-cationic Ag$_{12}$ nanocluster [(Cy-cAACP)$_6$Ag$_{12}$Cl$_3$](OTf)$_3$ (−132.2 (t, $J_{31P-109Ag}$ = 749.16 Hz) ppm).[17] The ^{31}P spectrum of the DCM-d_2 solution of **6** exhibited a broad triplet at −23.3 ppm ($J_{31P-109Ag}$ = 699.8 Hz) at rt, which was comparably downfield shifted than that of **5**, and previously reported [(Cy-cAACP)$_6$Ag$_{12}$Cl$_3$](OTf)$_3$.[17] The characteristic ^{31}P chemical shifts observed for **4–6** show that in each case, all four phosphorus atoms are having the same chemical environment in solution. Moreover, the much upfield shifted ^{31}P chemical shift values compared to those for the other cAAC=P$^−$ precursors: [cAAC=PK(THF)$_x$]$_n$ (**1**, 206.9 ppm), stibanyl-phosphaalkene (**2**, 49.1 ppm), and boryl-phosphaalkene (**3**, 28.6 ppm), clearly suggest the significant anionic nature of the phosphorus atoms in **4–6**.

The Cu(I)$_8$ NC [(Cy-cAACP)$_4$(Cu)$_4$(CuCl)$_4$] (**4**) crystallized in the monoclinic space group C2/c. The molecular structure of **4** is shown in **Figure 3**, which consists of four Cy-cAAC=P$^−$ anions, eight Cu(I) ions, and four Cl$^−$ ions (Figure 3). The central core of **4** possesses a near square planar Cu$^I_4$ unit [Cu-Cu-Cu 88.76/91.05°, Cu-P-Cu 73.52/73.30°]. Each Cu−Cu arm of the Cu$^I_4$ unit in **4** is bridged by a P atom of Cy-cAAC=P$^−$ anion, leading to the formation of a non-planar sheet of Cu$_4$P$_4$ unit with two P atoms on top/below it (0.46/0.55 Å). The average Cu−Cu and Cu−P distances are 2.64 and 2.207 Å,
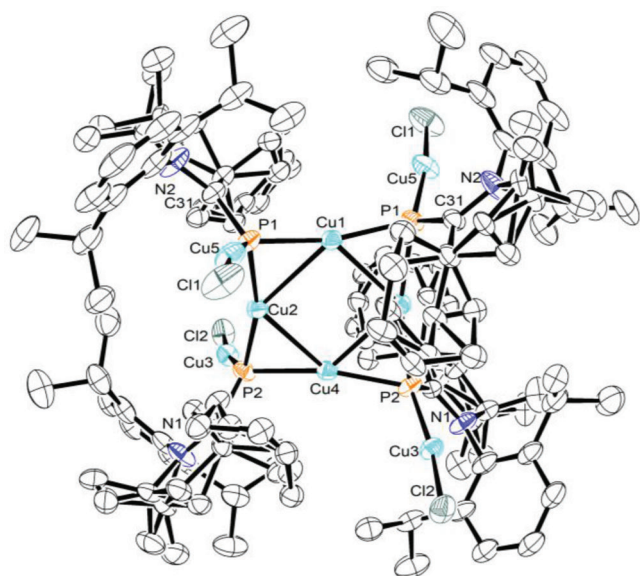
**ADVANCED
SCIENCE NEWS**

www.advancedsciencenews.com

**ADVANCED
OPTICAL
MATERIALS**

www.advopticalmat.de

Figure 3. Molecular structure of neutral Cu_8-cluster [(Cy-cAACP)$_4$(Cu)$_4$(CuCl)$_4$] (**4**). The ellipsoids are shown at the 50% probability level. Hydrogen atoms are omitted for clarity. Selected experimental bond lengths [Å] and bond angles [°]: Cu1-P1 2.2082(13), Cu1-Cu2 2.6416(8), P1-Cu5 2.1494(14), Cu5-Cl1 2.1081(16), Cu2-Cu4 2.6325(8), P1-Cu5-Cl1 170.17(7), P1-Cu2-P2 164.93(6), Cu4-Cu2-Cu1 91.04(2).

Figure 4. Molecular structure of neutral Ag_7-cluster [(Cy-cAACP)$_4$(Ag)$_4$(AgOTf)$_3$] (**5**). The ellipsoids are shown at the 50% probability level. Hydrogen atoms are omitted for clarity. Selected experimental bond lengths [Å] and bond angles [°]: Ag2-P3 2.5635 (10), Ag2-Ag3 3.0711(4), Ag2-P2 2.5312(10), Ag1-Ag3 2.8668(5), P1-Ag6 2.332(1), P2-Ag2-P3 131.10(3), Ag4-Ag2-Ag1 85.691(11), Ag1-P1-Ag3 72.52(3), Ag6-P1-Ag3 107.78(4).

respectively. The former is smaller in magnitude than that of the sum of van der Waals radii (2.8 Å), but significantly longer than those of original Cu(I)-mesityl complexes [2.46 Å],[25] $Cu(I)_2$[n] complexes [2.4521(3), 2.3899(7), 2.3870(6) Å; n = +1, 0, −1] containing μ-mesityl ligand on di-copper(I) with a PNNP ligand[26] and other Cu-clusters.[27] The shorter Cu1−Cu2 distance in **4** is assumed to be due to the cuprophilic interaction,[25] which is significantly shorter than the sum of van der Waals radii (2.8 Å). Such short Cu—Cu contacts suggest extensive luminescence behavior, as observed for other oligonuclear organo-[28–30] and amido-copper frameworks,[31,32] which has indeed been confirmed by the observation of a structureless emission band at ≈650 nm in the solid-state excitation spectrum of mesityl-copper complex (λ_{ex} >350 nm).[28] Given the short Cu–Cu distances in **4**, it was assumed that the emissive states are derived from the metal-centered d→s transitions of Cu^I, modified by Cu–Cu interactions. The P atom of each Cy-cAACP=P units of **4** is further bonded to a terminal Cu—Cl unit with an alternating up and down fashion around a non-planar sheet of Cu_4P_4 displaying a μ$_3$-bridging mode. The C—N bond length of Cy-cAAC in **4** is 1.325(6) Å, which is shorter than that of Cy-cAACPK (≈1.35 Å),[21] but longer than that of the free cAAC (≈1.30 Å) suggesting the formation of a partial C$_{cAAC}$−N double bond. The C$_{cAAC}$−P bond distance is 1.764(5)/1.759(5) Å, which is close to that of cAACP−Cl (≈1.73 Å).[22] These bond parameters suggest the bond between cAAC and P[−] anion of cAACP unit is a partial double bond [C$_{cAAC}$→P[−] / C$_{cAAC}$←P[−]].

To understand the bonding scenario, and electron densities distribution in **4**, we have performed natural bond orbital (NBO) analysis at BP86/LanL2DZ level of theory (see Supporting Information). The results from NBO analysis showed the polarized
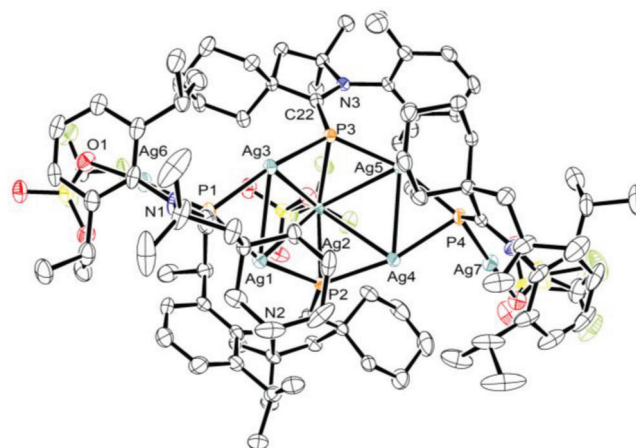
partial double bond nature of the C$_{cAAC}$—P bond given by the Wiberg bond index (WBI) of 1.25 (see Supporting Information). The WBI for a typical P—Cu bond of **4** ranging from 0.39 to 0.45 indicates a weaker bond. The Cu—Cl bonds are observed to be more polarized toward the Cl atoms having negative NBO charge, whereas Cu has a positive value of the NBO charge across the bond. The HOMO-LUMO energy gap of **4** was calculated to be 1.85 eV, which is reasonably larger, indicating a greater stability of **4**.

The $Ag(I)_7$ NC [(Cy-cAACP)$_4$(Ag)$_4$(AgOTf)$_3$] (**5**) crystallized in the monoclinic space group $P2_1/c$. The molecular structure (**Figure 4**) of **5** consists of seven Ag(I) ions, four Cy-cAAC=P[−] anions, and three OTf[−] ions. **5** possesses a non-planar and near rectangular Ag_4 core [Ag-Ag 2.8668(5)/2.8816(4), 4.22/4.23 Å]. Each of these four Ag(I) ions is bonded to a Cy-cAAC=P[−] anion. An Ag-OTf unit resides on the top of this non-planar rectangular Ag_4 unit to form an $Ag(I)_5$ unit [Ag-Ag 3.0711(4), 3.0145(4), 3.1903(4), 3.0402(4) Å]. All four Cy-cAAC=P units display a μ$_3$-bridging mode as seen in complexes **3/5**. The Ag—P—Ag bond angles around the central Ag_4 unit are 72.52/72.65° and 124.34/124.82°. The Ag−P distances are in the range of 2.3977(10) to 2.5635(10) Å. The overall non-planar tent-shaped Ag_7P_4 core of **5** possesses an Ag_5P_2 unit in the middle with two additional AgP units connected to shorter arms of the $Ag(I)_4$ rectangle. The average C—N and C—P distances of **5** are 1.32 and 1.76 Å, which are similar to those of **4**. The central Ag atom and two terminal Ag atoms of **5** are terminally bonded to triflate anion. NBO analysis of **5** at the BP86/LanL2DZ level of theory showed that the C$_{cAAC}$—P bond is evidently a single bond, given by the WBI of 0.97, and also more polarized toward the carbon atom. The central core bonds across Ag—P—Ag are primarily of 3-centered 2-electrons type bonds (see Supporting Information).

The HOMO of **5** corresponds to the C$_{cAAC}$=P π bond, delocalized toward the d-type orbital on the Ag atom bonded to the
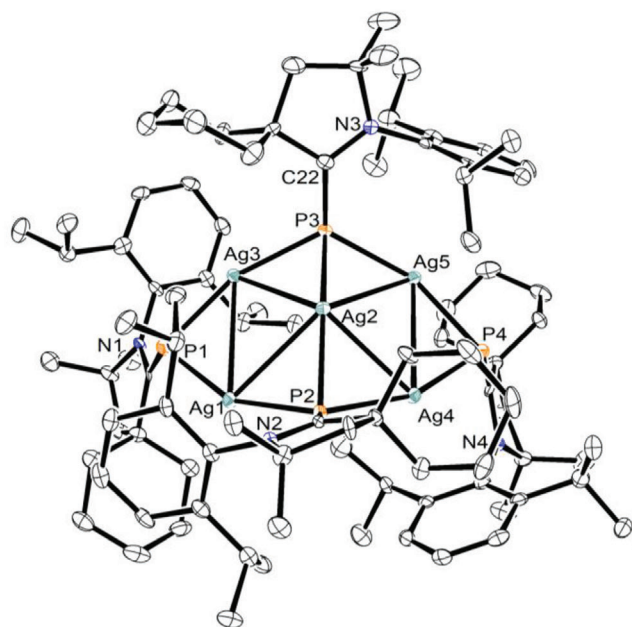
**ADVANCED
SCIENCE NEWS**

www.advancedsciencenews.com

**ADVANCED
OPTICAL
MATERIALS**

www.advopticalmat.de

Figure 5. Molecular structure of mono-cationic Ag$_5$-cluster [(Cy-cAACP)$_4$(Ag)$_5$]NTf$_2$ (**6**). The ellipsoids are shown at the 50% probability level. Hydrogen atoms, counter anion (NTf$_2$), and the lattice solvents (2 DCM) are omitted for clarity. Selected experimental bond lengths [Å] and bond angles [°]: Ag1-Ag2 3.0390(7), Ag2-Ag5 2.9960(7), Ag5-P4 2.3909(16), P4-Ag4 2.3922(16), Ag3-Ag2 2.8853(6), P1-Ag1 2.3708(16), Ag3-P1 2.3879(17), Ag1-P1-Ag3 86.22(5), Ag5-P4-Ag4 85.12(5), Ag1-Ag2-Ag4 91.558(17), Ag3-Ag2-Ag5 92.780(18), Ag1-Ag2-Ag3 66.531(16), Ag5-Ag2-Ag4 66.411(16).

same. The LUMO of **5** corresponds to the $\pi^{*}$$_{C=N}$ orbital of cAAC. The HOMO-LUMO energy gap for **5** was calculated to be 2.18 eV, which is reasonably larger, indicating greater stability of the NC.

The non-planar tent-like Ag(I)$_5$P$_4$ core of the mono-cationic complex [(Cy-cAACP)$_4$(Ag)$_5$]NTf$_2$ (**6**) can be compared with the core of complex **5** with a significant change in the bond parameters (**Figure 5**). The Ag(I) ion, residing at the top pole position in **6**, is 1.26 Å above the average Ag$_4$ plane, which is significantly shorter than that of **5** [1.71 Å] with an Ag−Ag distance of 2.96 Å [3.0390(7), 2.8853(6), 2.9099(6), 2.9960(7) Å], which is slightly shorter than that of **5** [3.08 Å]. Two P−Ag bond distances [≈2.54 Å] in **6** [from P to the Ag(I) atom at the top pole position] are slightly longer than those of **5** [2.49 Å], while the other P-Ag distances of **6** are very similar to those of **5**. The Ag−P−Ag bond angle [85.11/86.22°] around two μ-P bridges is significantly wider than those [72.52/72.65°] of **5**, which is a consequence of Ag(I) at the top position coming closer to the Ag$_4$ plane without any coordination from any anion. The average C-N, and C-P distances of **5**/**6** are 1.32/1.33 and 1.76/1.74 Å, which are similar to those of **4**. The central Ag atom and the two terminal Ag atoms of **5** are terminally bonded to the triflate anion. The metal ions of three complexes (**4**–**6**) are bonded to each other in closer proximity due to corresponding metallophilic interactions, which are known to stabilize the complexes by nearly 7 kcal mol^{-1}.[28–32] The NBO analysis of **6** performed at the BP86/LanL2DZ level of theory deciphers the C$_{cAAC}$-P bond evidently as a partial double bond (WBI of 1.38) with the σ bond polarized toward the carbene

carbon, and the π bond polarized toward the P (see Supporting Information).

The bonds across the central Ag-P-Ag core are primarily of 3-centered 2-electron type (observed across Ag1-Ag2-P7, Ag3-Ag5-P8 centers), where the three atomic species (two Ag, and one P atom) provide a stabilizing effect. The P atom contributes majorly (86%) to this stabilization with minor contributions from the Ag atoms. The HOMO of **6** is a p-type orbital representing the lone pairs on the two P atoms, and the LUMO corresponds to the $\pi^{*}$$_{C=N}$ of cAAC as observed in both the NCs **4**, and **5** (see Supporting Information).

The stability of the NCs **4**–**6** in the solid state was studied by the thermogravimetric analysis (for TGA see Supporting Information). The solid powder of **4** was exposed to air at rt for 24 h without any significant decomposition, which was also confirmed by the NMR spectroscopic measurements of the respective air-exposed samples. However, the powder of **5** and **6** decomposed after 12 h of exposure to air to a brown solid, which could not be characterized further by NMR studies.

The stability of the NCs [(Cy-cAACP)$_4$(Cu)$_4$(CuCl)$_4$] (**4**), [(Cy-cAACP)$_4$(Ag)$_4$(AgOTf)$_3$] (**5**), and [(Cy-cAACP)$_4$(Ag)$_5$]NTf$_2$ (**6**) in DCM solution was further confirmed by ESI-MS spectrometry (**Figure 6**; Figure S60, Supporting Information). There were no additional signals observed in the ^{31}P NMR spectra of the respective DCM-d_2 solutions of the NCs **4**–**6** upon aerial exposure for ≈30 min to 1 h.

2.1. Photophysical Properties

The solid powder, and DCM solutions of NCs **4**, and **6** were found to be bright luminescent, emitting red to orange light under a laboratory UV lamp of 365 nm wavelength at rt, and at 77 K (liquid nitrogen bath, see Supporting Information). On the other hand, the DCM solution of **5** was observed to emit green light at rt, and bright yellow light at 77 K (liquid nitrogen bath) under the laboratory UV lamp of 365 nm wavelength (see Supporting Information). Fascinated by these initial luminescence studies, we performed detailed investigations of the photophysical properties for all the NCs **4**–**6** (Figures 7–13; see Figures S8–S22, Supporting Information).

The UV–vis absorption spectrum of a DCM solution of **4** was recorded at rt (300 K) under an argon atmosphere, which showed the absorption maximum (λ_{max}) at 411 nm with a shoulder at 344 nm, and a less intense band between 550 and 650 nm (**Figure 7**, blue line). Similarly, the DCM solutions of **5**, and **6** exhibited absorption maxima (λ_{max}) at comparatively higher energy wavelengths of 370 (Figure 7, red line), and 357 nm (Figure 7, green line), respectively, at 300 K under an argon atmosphere. The above UV–vis studies revealed that the higher the nuclearity of the cluster, the higher the wavelength of the absorption bands. The time-dependent density functional theory (TD-DFT) calculations performed at BP86/LanL2DZ level of theory on **4** inferred a well-resolved calculated absorption band in its neutral singlet state at 412.3 nm, composed of four major excitations ≈3.01–3.02 eV along with a weaker absorption at 353.6 nm having relatively highest oscillator frequencies of $f = 0.0037$, and $f = 0.0128$, respectively (see Supporting Information). These values are in very good agreement with the experimentally observed
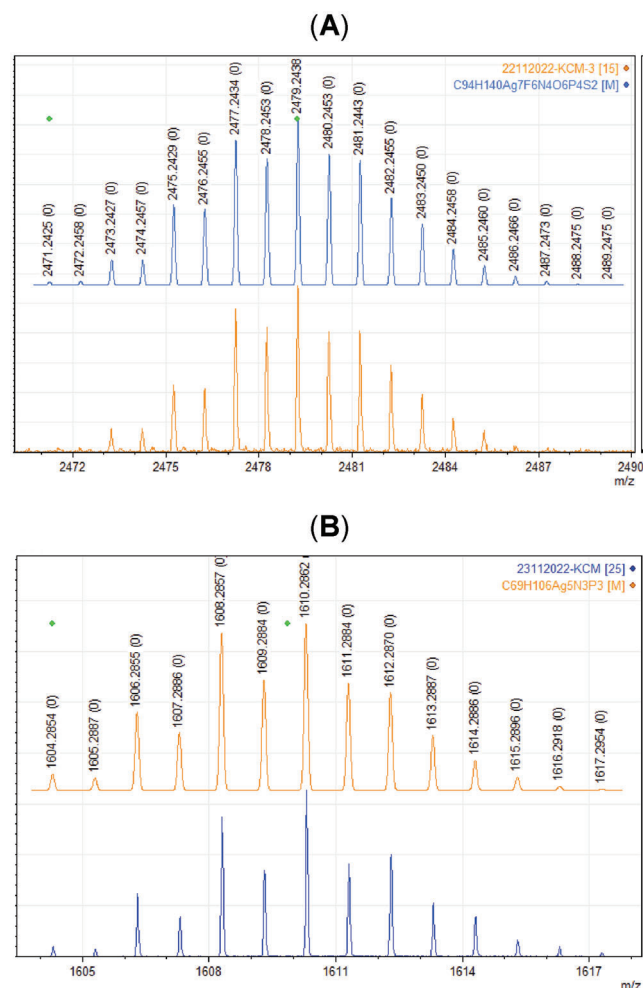
**ADVANCED
SCIENCE NEWS**

www.advancedsciencenews.com

**ADVANCED
OPTICAL
MATERIALS**

www.advopticalmat.de

Figure 6. A) Experimental (bottom) and simulated (top) ESI-MS spectra of $(Cy\text{-}cAACP)_4Ag_7(OTf)_2$ mono-cation of **5**. $Cy\text{-}cAACP = C_{23}H_{35}NP$, $OTf = CF_3SO_3$. B) Experimental (bottom) and simulated (top) ESI-MS mass spectra of $[(Cy\text{-}cAACP)_3Ag_5 + H]$ cation of **6**. $Cy\text{-}cAAC = C_{23}H_{35}NP$. See Supporting Information for the ESI-MS spectrum of $[(Cy\text{-}cAACP)_4(Cu)_4(CuCl)_4]$ **(4)**.

Figure 7. UV–vis absorption spectra of $[(Cy\text{-}cAACP)_4(Cu)_4(CuCl)_4]$ **(4)**, $[(Cy\text{-}cAACP)_4(Ag)_4(AgOTf)_3]$ **(5)**, and $[(Cy\text{-}cAACP)_4(Ag)_5](NTf_2)$ **(6)** in DCM solution at rt. The absorption maximum (λ_{max}) was observed at 411, 370, and 357 nm, respectively.

Figure 8. Left: UV–vis absorption spectrum of $[(Cy\text{-}cAACP)_4(Cu)_4(CuCl)_4]$ **(4)** in solid state at rt. The absorption maximum (λ_{max}) was observed at 450 nm. Right: Powder of $[(Cy\text{-}cAACP)_4(Cu)_4(CuCl)_4]$ **(4)** under white light (top), under short UV at 254 nm (middle), and under long UV at 365 nm (bottom) at rt.

absorption wavelengths (Figure 7). TD-DFT calculations showed that the above absorptions of **4** correspond to the electronic transition from HOMO-8→LUMO+4, i.e., from the d_z^2 type orbital on Cu atom with lone pair contribution from the chlorine (HOMO-8) into the $\pi^*_{C=N}$ (LUMO+4) of cAAC. This confirms the metal-to-ligand charge transfer (MLCT)[14k,16b] in **4**.

On the other hand, TD-DFT calculations on **6** revealed that the λ_{max} corresponds to the transition of HOMO-3→LUMO+6, i.e., from the $\pi_{CcAAC=P}$ bond, which is delocalized over the d-type orbital on Ag atom to the π^* orbital of the phenyl ring of the Dip group (Dip = diisopropylphenyl) of cAAC.

The UV–vis absorption spectrum of the pure crystals and/or powder of **4** exhibited a broad band ranging from 300 to 800 nm approximately with the λ_{max} at 450 nm (**Figure 8**).

The photoluminescence (PL) spectrum of DCM solution of **4** at 300 K exhibited a bright red emission with λ_{em} of 683 nm (see Supporting Information).
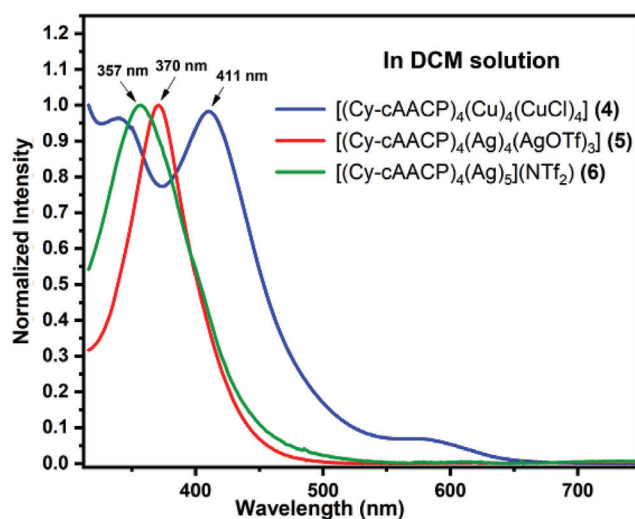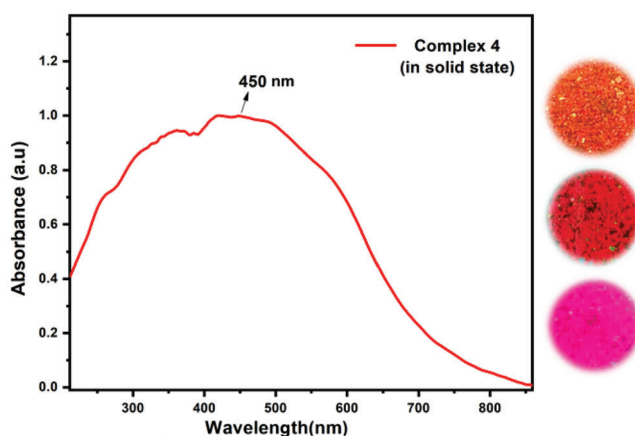
The PL spectrum of the powder samples of pure crystals of Cu_8 nanocluster **4** at 300 K exhibited an intense red emission band at 680 nm (λ_{em}), analogous to that observed in the solution with a high photoluminescence quantum yield (PLQY), Φ_{PL} of 20%, and a considerably higher average lifetime (τ) of 26.3 µs (see Supporting Information), indicating a spin-forbidden intersystem crossing (ISC), which can very often lead to an exciting light emitting material with thermally activated delayed fluorescence (TADF) with a real-time application in OLED generation.

To have a vivid understanding of the excited state transitions, we recorded the PL spectra of the powder of pure crystals of **4** at various temperatures ranging from 80 to 300 K (**Figure 9**). A gradual increase in the intensity of the PL spectra was observed by increasing the temperature from 80 K ($\lambda_{em} = 760$ nm) to 300 K ($\lambda_{em} = 680$ nm) along with a red shift of λ_{em} of ≈80 nm going

**ADVANCED
SCIENCE NEWS**

www.advancedsciencenews.com

**ADVANCED
OPTICAL
MATERIALS**

www.advopticalmat.de

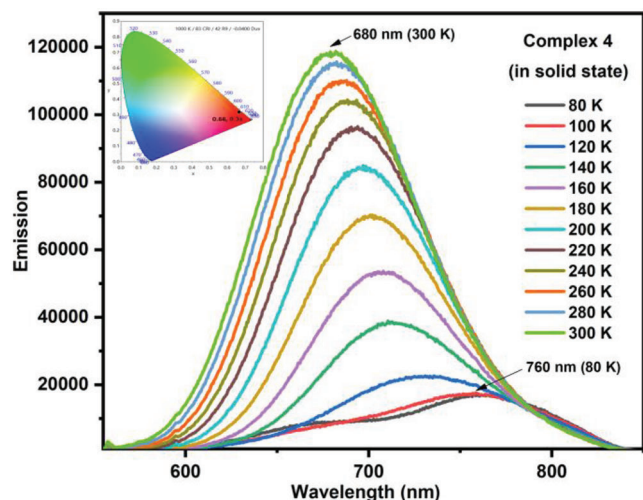**Figure 9.** Temperature-dependent photoluminescence (PL) spectra of $[(Cy\text{-}cAACP)_4(Cu)_4(CuCl)_4]$ (**4**) in solid state. Inset: The PL color coordinates of **4**, plotted in the CIE 1931 chromaticity diagram. The blue dot corresponds to the coordinates attributed to pure red-light emission (0.68, 0.31).
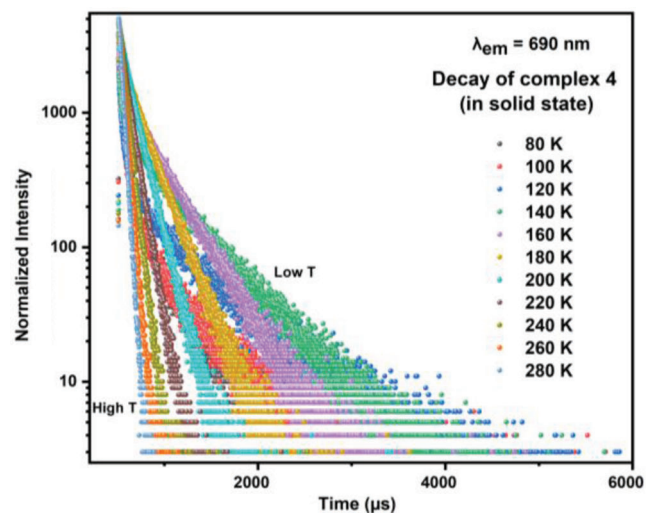

Figure 11. Lifetime versus temperature plot for $[(Cy\text{-}cAACP)_4(Cu)_4(CuCl)_4]$ (**4**) in solid state (λ_{em} = 690 nm).

Figure 10. Temperature dependent decay plot of $[(Cy\text{-}cAACP)_4(Cu)_4(CuCl)_4]$ (**4**) in solid state at λ_{em} = 690 nm, and λ_{ex} = 450 nm.
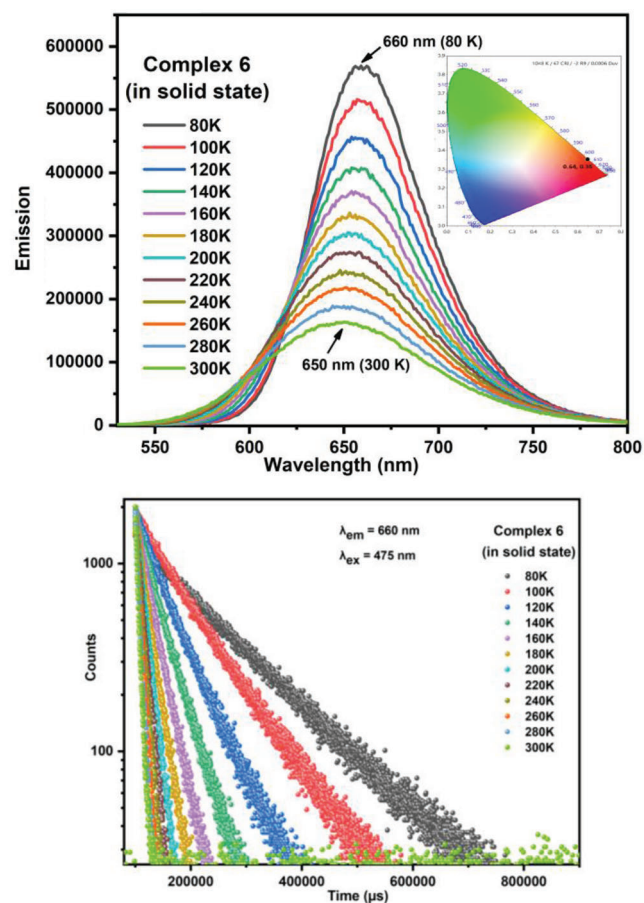
Figure 12. Top: Temperature-dependent photoluminescence (PL) spectra of $[(Cy\text{-}cAACP)_4(Ag)_5](NTf_2)$ (**6**) in solid-state on excitation at 445 nm. Bottom: Temperature dependent decay plot of $[(Cy\text{-}cAACP)_4(Ag)_5](NTf_2)$ (**6**) in solid-state at (λ_{em} = 660 nm and λ_{ex} = 475 nm).

down from rt to the 80 K (Figure 9).[14i–j] Considering the fact that TADF is ruled out at a very low temperature (80 K), it is assumed that only the energetically lower-lying phosphorescence prevails at 80 K.

The temperature-dependent decay plots of the same sample of **4** showed a bi-exponential nature with around ten-fold increase in the average lifetime, τ from 26.3 (at 300 K) to 267.15 (at 80 K) µs, suggesting that the emission in the solid state originates from two different excited states, i.e., S_1 and T_1, which are in thermal equilibrium (**Figure 10**). For such thermally equilibrated excited states S_1, and T_1; the temperature dependence of the emission
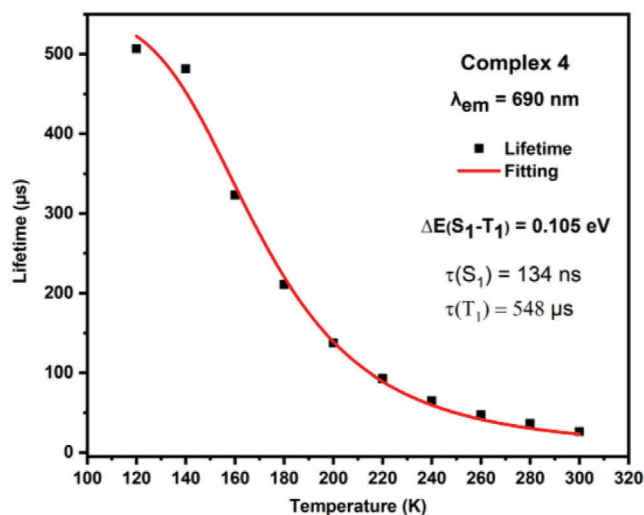
**ADVANCED
SCIENCE NEWS**
www.advancedsciencenews.com

**ADVANCED
OPTICAL
MATERIALS**
www.advopticalmat.de

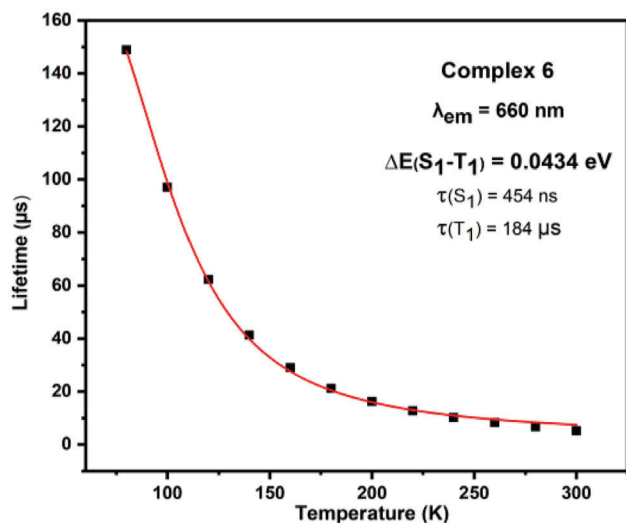**Figure 13.** Plot of emission lifetime at 660 nm against various temperatures for $[(Cy\text{-}cAACP)_4(Ag)_5](NTf_2)$ **(6)**.

Figure 14. Cyclic voltammograms of the nanocluster $[(Cy\text{-}cAACP)_4(Cu)_4(CuCl)_4]$ **(4)** in DCM containing 0.1 M $[n\text{-}Bu_4N]PF_6$ as the electrolyte (CE: Pt, WE: GC, RE: Ag).

decay time can be expressed by the following Boltzmann equation (Equation 1) derived from the TADF model.[33]

$$\tau_{av} = \frac{3 + \exp\left[\frac{-\Delta E(S_1-T_1)}{k_B T}\right]}{\frac{3}{\tau(T_1)} + \left[\frac{1}{\tau(S_1)}\right]\exp\left[\frac{-\Delta E(S_1-T_1)}{k_B T}\right]} \quad (1)$$

Where τ represents the experimental average lifetime, K_B is the Boltzmann constant, and T is the absolute temperature. The individual lifetime decay for singlet and triplet lowest excited states are given by, $\tau(S_1)$ and $\tau(T_1)$, respectively. The $\Delta E(S_1\text{-}T_1)$ corresponds to the energy difference between the S_1 and T_1 states. For an effective TADF to be in place, the $\Delta E(S_1\text{-}T_1)$ should preferably have a value less than 0.37 eV.[34] The fits of the temperature-dependent PL decay curve to Equation 1 gave the $\Delta E(S_1\text{-}T_1) = 0.105$ eV (coefficient of determination, COD, $(R)^2 = 0.995$).

The radiative lifetimes for **4** derived from the fit to Equation 1 were found to be $\tau(S_1) = 134$ ns, $\tau(T_1) = 548$ μs, **(Figure 11)**.

The fitted $\tau(T_1)$ value for **4** was observed to be very close to the experimentally obtained value of 507 μs at 120 K, which was comparable ($\tau(S_1) = 150 \pm 15$ ns) with the values reported by Hamze et al. in 2019 for the cAAC-Cu-amide.[16b] For the $Cu(I)_8$ NC **4**, the emissions at lower temperatures are assumed to be mostly of a phosphorescence nature. The radiative rate constant of TADF ($k(S_1)$) was calculated to be 0.75×10^4 s^{-1}. The significantly lower singlet-triplet energy gap and all other calculated and/or experimentally observed photophysical parameters unambiguously point toward the TADF nature of the Cu_8 nanocluster **4**.[35–37]

Similar photophysical studies have also been performed for $Ag(I)_7$ **(5)**, and $Ag(I)_5$ **(6)** NCs (see Supporting Information). The temperature-dependent PL spectra of **5** in DCM solution showed a redshift of the λ_{em} values of ≈17 nm with a considerable increase in the emission intensity by lowering the temperature from 300 K ($\lambda_{em} = 560$ nm, $\tau = 60.48$ μs) to 200 K ($\lambda_{em} = 577$ nm, $\tau = 285$ μs). The radiative rate constant of TADF ($k(S_1)$) was calculated to be 1.65×10^4 s^{-1}. The PLQY, Φ_{PL} was found to be 2.71%
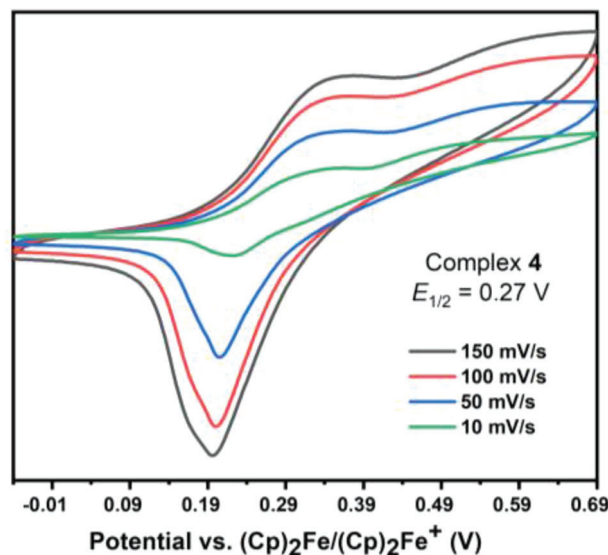
in DCM solution. To establish the nature of the emission for **5**, we calculated the energy gap between the singlet and triplet excited states by fitting the lifetime versus temperature plot to the Boltzmann equation (Equation 1) with values of $\tau(S_1) = 0.26$ ns, $\tau(T_1) = 278.8$ μs, and the $\Delta E(S_1\text{-}T_1)$ was found to be 0.30 eV, which is well within the range of TADF.[34]

The rt PL spectrum of **6** showed an intense red emission with λ_{em} of 650 nm with a comparably higher average lifetime, τ of 5.26 μs at rt, and the PLQY, Φ_{PL} of 6% (**Figure 12**, Top).

To investigate the mechanism of the excited state emission taking place in **6**, we recorded the temperature-dependent emission and the decay times ranging from 80 to 300 K in the solid state (Figure 12, Bottom). The temperature-dependent PL spectra of **6** (Figure 12, Top) showed a similar pattern as that of **5** with a redshift in the λ_{em} values of 10 nm, while raising the temperature from 80 to 300 K with a steady decrease in the lifetime, τ from 149 to 5.26 μs. The fitting of the experimental temperature-dependent decay data to the Boltzmann equation (Equation 1) afforded the values of $\tau(S_1) = 454$ ns, $\tau(T_1) = 184$ μs, and $\Delta E(S_1\text{-}T_1) = 0.0434$ eV (with an $(R)^2$ (COD) of 0.999), once again confirming that the emission in **6** is due to the delayed fluorescence. However, the reduced emission intensity for both the Ag NCs **5** and **6** at rt can be attributed to the higher rate of non-radiative decay compared to that of the radiative decay, which was also confirmed by the respective k_r and k_{nr} values calculated (For **5**: $k_r = 0.044 \times 10^4$ s^{-1}, $k_{nr} = 1.57 \times 10^4$ s^{-1}; for **6**: $k_r = 1.14 \times 10^4$ s^{-1}, $k_{nr} = 1.575 \times 10^5$ s^{-1}) (**Figure 13**).

The redox properties of the NCs **4–6** were studied by the cyclic voltammetry (CV) analyses in DCM solution, using 0.1 M solution of $[n\text{-}Bu_4N]PF_6$ as the electrolyte (see Supporting Information). The cyclic voltammograms of the $Cu(I)_8$ NC $[(Cy\text{-}cAACP)_4(Cu)_4(CuCl)_4]$ **(4)** exhibited a near quasi-reversible oxidation process at 0.27 V (**Figure 14**; see Supporting Information for the CV of NCs **5** and **6**).

ADVANCED
SCIENCE NEWS
www.advancedsciencenews.com

ADVANCED
OPTICAL
MATERIALS
www.advopticalmat.de

2.2. Catalytic Property of 4

Driven by the unique TADF property of the redox-active Cu(I)$_8$ NC **4** having the largest PLQY of 20% among the three NCs **4–6**, we decided to investigate the photocatalytic activity of this species under ambient conditions. In general, a redox-active photocatalyst (PC) can be defined as a light-absorbing material, which uses light as the source of energy for increasing the rate of a reaction. A PC accesses its excited state, PC* upon absorption of light, from where either photoinduced energy transfer and/or photoinduced electron transfer can take place between PC* and the substrate molecule. Since 2007, there have been huge efforts put forward in order to develop novel photoactive organometallic complexes to mediate various organic transformations under ambient reaction conditions. In this regard, the pioneering demonstrations depicted by the research groups of MacMillan, Yoon, and Stephenson are noteworthy.[38] The long excited-state lifetime of the neutral Cu$_8$ nanocluster **4** suggested that it may serve as an earth-abundant photocatalyst. Considering the literature precedence for Cu(I)-based catalysts involved in carbene transfer reactions, we decided to study the photocatalytic activity of nanocluster **4** for the C2-C3 cyclopropanation of N-protected indoles.[39] We commenced our studies by choosing N-pyrimidyl indole (**7a**) and methyl-2-diazo-2-phenylacetate (**9a**) as model substrates to react at rt using DCM as a solvent in the presence of 0.1 mol% of the TADF nanocluster **4** (see Table S18, Supporting Information, entry 1) under blue LED (456 nm).

To our delight, after 2 h, the C2-C3 cyclopropanated N-pyrimidyl indole **10a** was obtained as a single diastereomer (*exo-*) in 81% isolated yield. With this initial result, we moved to optimize the reaction condition (Table S18, Supporting Information). Upon increasing the catalyst loading to 1 mol% under blue LED (456 nm) at rt, using DCM as the solvent resulted in the formation of the desired product **10a** in 94% yield. Control experiments have been performed by replacing the NC **4** using only blue LED, keeping other reaction conditions the same. After 24 h, no conversion was observed, and the starting material **7a** was re-isolated from the reaction mixture with quantitative yield. Having the optimized reaction condition in hand, we probed the generality of this photocatalytic reaction by varying the indoles **7** and diazoesters **9** (**Scheme 4**). In all the cases, the *exo*-diastereomers of the desired cyclopropanated products (**10b-10i**) were obtained exclusively in good to excellent yields (26–96%). Moving to the un-activated olefins, e.g., the styrenes (**8**); the optimized reaction conditions afforded the desired cyclopropanated products (**11a-11i**) with good yields (43–84%) and excellent diastereoselectivity. The relative stereochemistry of the cyclopropanated products: **10**, and **11** was unambiguously established by single-crystal X-ray diffraction (Scheme 4, see Figures S97–S99, Supporting Information). Carrying out the catalytic cyclopropanation under similar reaction conditions, replacing the blue LED with a green LED (530 nm) resulted in reduced yields of the corresponding cyclopropanated products. For example, under optimized reaction conditions in the presence of green LED, reaction of 4-methoxy styrene (**8a**), and methyl 2-diazo-2-phenylacetate (**9b**) afforded the cyclopropanated product **11a** after 2 h with a lower yield of 55% as compared to that of 70%, which was obtained previously in presence of Blue LED.
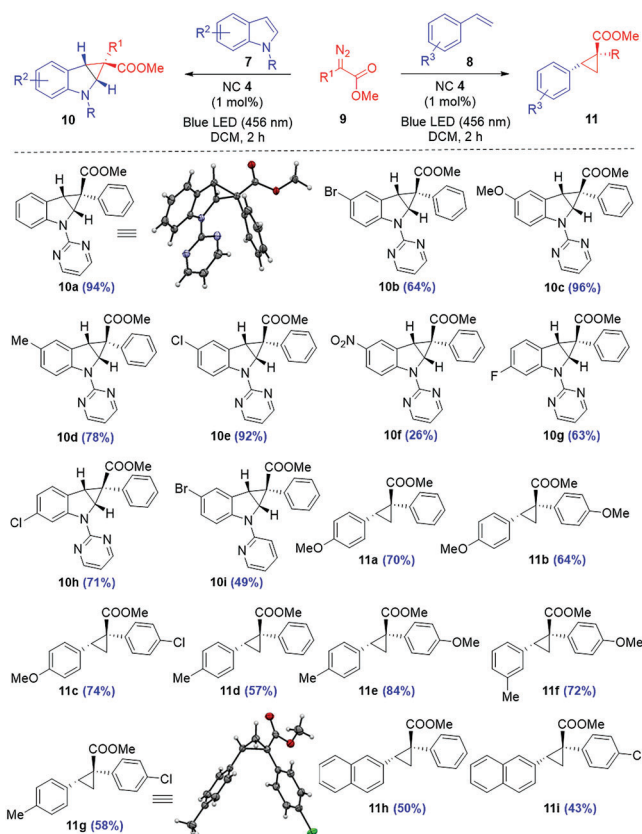
Scheme 4. [(Cy-cAACP)$_4$(Cu)$_4$(CuCl)$_4$] (**4**)-catalyzed stereoselective cyclopropanation of substituted indoles and styrenes in the presence of diazoesters.

3. Conclusion

In conclusion, we have successfully synthesized three novel oxygen, and moisture-tolerant coinage metal(I) nanoclusters (NCs) (with average diameters of 1.6–2 nm) with Cu$_8$ (**4**), Ag$_7$ (**5**), and Ag$_5$ (**6**) metallic cores stabilized by cyclic alkyl(amino) carbene (cAAC)-supported monoanionic phosphorus as the ligand. The structural elucidations of all the atomically precise NCs have been established by NMR, ESI-MS, and single-crystal X-ray diffraction. The PL spectra of **4**, **5**, and **6** in the solid-state exhibited intense red to yellow to orange emission, and high photoluminescence quantum yield (PLQY) of up to 20% at room temperature (rt) with considerably higher average lifetimes (τ) of 26.3, 60.48, and 5.26 µs, respectively, indicative of the thermal equilibrium between the triplet excited state (T_1) and the lowest energy singlet excited state (S_1). The observed red shift of the emission maxima for the temperature-dependent PL spectra of **4**, **5**, and **6** within a temperature range of 300–80 K, and the smaller $\Delta E(S_1\text{-}T_1)$ values confirm the thermally activated delayed fluorescence (TADF) nature of all the reported NCs. Together with the improved stability of the NCs by careful utilization of the unusual ligand field of cAAC=P$^-$, and sufficient solubility in organic solvents may find them potential applications for the fabrication of inorganic and organic light emitting diodes (LEDs). Furthermore, we have shown that the TADF nature of the redox active photocatalyst Cu(I)$_8$ nanocluster **4** can be efficiently utilized as

the novel photocatalyst for the stereoselective cyclopropanation of N-protected indoles, and unactivated styrenes by carbene transfer reactions from the respective diazoesters with excellent yields. This work brings the first example of cAAC-phosphinidenide being utilized as the excellent stabilizing ligand for the generation of redox-active Cu(I), and Ag(I) NCs exhibiting TADF properties with further application of the former as the efficient photo-redox catalyst.

4. Experimental Section

Crystallographic Details: The single-crystal X-ray data for **4**–**6** were collected on a Bruker D8 VENTURE diffractometer equipped with PHOTON III C28 detector using IμS 3.0 microfocus sealed X-ray source with Molybdenum Kα ($\lambda = 0.71073$ Å) radiation. A complete data set was collected following the strategies generated using the APEX4 [40] module of the Bruker software suite. The data reduction was carried out using SAINTPLUS,[40] and multi-scan absorption correction was performed using the program SADABS.[41] The crystal structures were solved by the intrinsic phasing method (SHELXT)[42] and were refined with full-matrix least squares on F^2 using ShelXle[43] plug-in included in APEX4. All non-hydrogen atoms were refined anisotropically. Crystallographic Information Files can be obtained free of charge from the Cambridge Crystallographic Data Centre via www.ccdc.cam.ac.uk/structures/, using the Deposition Numbers 2149753 (for **4**), 2194457 (for **5**), 2242237 (for **6**).

Photophysical Studies: All photophysical studies were performed under an argon atmosphere using standard quartz cuvettes (1 cm x 1 cm cross-section) with pure crystals of **4**–**6**. The UV–vis absorption spectra were recorded using Agilent Cary Series UV–vis–NIR spectrophotometers. The emission, lifetime, and absolute quantum yield measurements of **4**–**6** in solution and/or solid states were recorded on EDINBURGH FLS1000 photoluminescence spectrometer, attached with an Optistat DN cryostat.

General Procedure for Photocatalytic C2-C3 Cyclopropanation of Aromatic Heterocycles: A mixture of N-pyrimidyl-indole, **1** (0.1 mmol), and **[(Cy-cAACP)₄(Cu)₄(CuCl)₄]** complex **4** (0.5 mg, 1 mol%) were taken in an oven dried reaction vial. To this, 1 mL of dry DCM was added with vigorous stirring under an argon atmosphere. Thereafter, the reaction flask was cooled to 0 °C. To this, a solution of the diazoester derivative **9a** (0.13 mmol) in 1 mL of dry DCM was added dropwise under an argon atmosphere over a period of 20 min. Afterward, the reaction mixture was irradiated in Blue LED (456 nm) and then allowed to stir for the next 2 h. After completion of the reaction, as monitored by TLC, DCM was evaporated by using a rotary evaporator under reduced pressure, and the crude solid was purified by column chromatography on silica gel (230–400 μm) with hexane/EtOAc as an eluent to afford the desired cyclopropanated product **10a** as a white solid in 94% yield. R_f = 0.53 (Hex/EA = 10:3); **MP**: 216–219 °C; **¹H NMR** (400 MHz, CDCl₃, ppm) δ: 8.56 (d, J = 4 Hz, **2H**, Ar*H*), 7.97 (d, J = 8 Hz, **1H**, Ar*H*), 7.45 (d, J = 8 Hz, **1H**,Ar*H*), 7.04 (t,J = 8 Hz, **1H**,Ar*H*), 7.00–6.94 (m, **1H**,Ar*H*), 6.91 (t,J = 8 Hz, **3H**,Ar*H*), 6.84 (dd,J = 12, 4 Hz, **3H**,Ar*H*), 5.40 (d, J = 4 Hz, **1H**), 3.86 (d, J = 8 Hz, **1H**), 3.70 (s, **3H**,—CO₂C*H₃*); **¹³C NMR** (101 MHz, CDCl₃, ppm) δ: 174.3, 157.9, 142.9, 132.4, 130.8, 129.7, 127.8, 127.6, 127.2, 125.5, 121.8, 115.6, 113.2, 52.9, 51.9, 35.5, 32.1; **FT-IR**v_{max} (neat)/cm⁻¹: 3028.83, 2950.88, 1605.63, 915.03, 1090.49, 984.21, 863.48, 997.25, 1075.84, 679.09, 1023.42, 1157.17, 1342.9, 1118.52, 968.19, 1387.92; **HRMS** (ESI): m/z calculated for C₂₁H₁₈N₃O₂ [M+H]⁺ 344.1399, found: 344.1509. Detailed synthetic procedures and analytical data of complexes **4**–**6** are provided in the Supporting Information.

Supporting Information

Supporting Information is available from the Wiley Online Library or from the author.

[1] a) H. Uoyama, K. Goushi, K. Shizu, H. Nomura, C. Adachi, *Nature* **2012**, *492*, 234. b) Q. Zhang, J. Li, K. Shizu, S. Huang, S. Hirata, H. Miyazaki, C. Adachi, *J. Am. Chem. Soc.* **2012**, *134*, 14706. c) F. B. Dias, K. N. Bourdakos, V. Jankus, K. C. Moss, K. T. Kamtekar, V. Bhalla, J. Santos, M. R. Bryce, A. P. Monkman, *Adv. Mater.* **2013**, *25*, 3707.

[2] a) M. Osawa, I. Kawata, R. Ishii, S. Igawa, M. Hashimoto, M. Hoshino, *J. Mater. Chem. C* **2013**, *1*, 4375. b) S. Igawa, M. Hashimoto, I. Kawata, M. Yashima, M. Hoshino, M. Osawa, *J. Mater. Chem. C* **2013**, *1*, 542. c) J. C. Deaton, S. C. Switalski, D. Y. Kondakov, R. H. Young, T. D. Pawlik, D. J. Giesen, S. B. Harkins, A. J. M. Miller, S. F. Mickenberg, J. C. Peters, *J. Am. Chem. Soc.* **2010**, *132*, 9499. d) M. Hashimoto, S. Igawa, M. Yashima, I. Kawata, M. Hoshino, M. Osawa, *J. Am. Chem. Soc.* **2011**, *133*, 10348. e) F.-S. Guo, B. M. Day, Y.-C. Chen, M.-L. Tong, A. Mansikkamäki, R. A. Layfield, *Science* **2018**, *362*, 1400.

[3] M. A. Bryden, E. Zysman-Colman, *Chem. Soc. Rev.* **2021**, *50*, 7587.

[4] a) X. Kang, M. Zhu, *Chem. Soc. Rev.* **2019**, *48*, 2422. b) R. Jin, C. Zeng, M. Zhou, Y. Chen, *Chem. Rev.* **2016**, *116*, 10346. c) M. Chen, Z. Lei, W. Feng, C. Li, Q.-M. Wang, F. Li, *Biomaterials* **2013**, *34*, 4284. d) H. Yu, B. Rao, W. Jiang, S. Yang, M. Zhu, *Coord. Chem. Rev.* **2019**, *378*, 595.

[5] a) C. A. Parker, in *Advanced in Photochemistry*, (Eds.: W. A. Noyes Jr., G. S. Hammond, J. N. Pitts Jr.), John Wiley & Sons, Inc., New Jersey, USA **1964**, Vol. *2*, pp. 305–383. b) G. Blasse, D. R. McMillin, *Chem. Phys. Lett.* **1980**, *70*, 1. c) D. Felder, J.-F. Nierengarten, F. Barigelletti, B. Ventura, N. Armaroli, *J. Am. Chem. Soc.* **2001**, *123*, 6291. d) H. Yersin, A. F. Rausch, R. Czerwieniec, T. Hofbeck, T. Fischer, *Coord. Chem. Rev.* **2011**, *255*, 2622. e) H. Yersin, A. F. Rausch, R. Czerwieniec, in *Physics of Organic Semiconductors*, (Eds.: W. Bruettig, C. Adachi, R. J. Holmes), 2nd Ed, Wiley-VCH, Weinheim **2012**, pp. 371–424.

[6] a) S. F. Yuan, P. Li, Q. Tang, X. K. Wan, Z. A. Nan, D. E. Jiang, Q. M. Wang, *Nanoscale* **2017**, *9*, 11405. b) Y. Yang, T. Jia, Y. Z. Han, Z. A.

ADVANCED
SCIENCE NEWS

www.advancedsciencenews.com

ADVANCED
OPTICAL
MATERIALS

www.advopticalmat.de

Nan, S. F. Yuan, F. L. Yang, D. Sun, *Angew. Chem., Int. Ed.* **2019**, *58*, 12280; c) Y. Yang, T. Jia, Y. Z. Han, Z. A. Nan, S. F. Yuan, F. L. Yang, D. Sun, *Angew. Chem.* **2019**, *131*, 12408.

[7] a) X. Liu, W. W. Xu, X. Y. Huang, E. D. Wang, X. Cai, Y. Zhao, J. Li, M. Xiao, C. F. Zhang, Y. Gao, W. P. Ding, Y. Zhu, *Nat. Commun.* **2020**, *11*, 3349. b) Q. F. Yao, Z. N. Wu, Z. H. Liu, Y. Z. Lin, X. Yuan, J. P. Xie, *Chem. Sci.* **2021**, *12*, 99.

[8] Z. Wang, R. K. Gupta, G. G. Luo, D. Sun, *Chem. Rec.* **2020**, *20*, 389.

[9] Z.-H. Pan, C.-L. Deng, Z. Wang, J.-Q. Lin, G.-G. Luo, D. Sun, *CrystEng-Comm* **2020**, *22*, 3736.

[10] a) X. T. Shen, X. L. Ma, Q. L. Ni, M. X. Ma, L. C. Gui, C. Hou, R. B. Hou, X. J. Wang, *Nanoscale* **2018**, *10*, 515. b) X. T. Yuan, C. F. Sun, X. H. Li, S. Malola, B. K. Teo, H. Hakkinen, L. S. Zheng, N. F. Zheng, *J. Am. Chem. Soc.* **2019**, *141*, 11905.

[11] a) Z. Wang, H. T. Sun, M. Kurmoo, Q. Y. Liu, G. L. Zhuang, Q. Q. Zhao, X. P. Wang, C. H. Tung, D. Sun, *Chem. Sci.* **2019**, *10*, 4862. b) K. G. Liu, X. M. Gao, T. Y. Liu, M. L. Hu, D. E. Jiang, *J. Am. Chem. Soc.* **2020**, *142*, 16905. c) T. Y. Liu, D. E. Jiang, *J. Chem. Phys.* **2021**, *155*, 16905.

[12] S. F. Yuan, Z. J. Guan, W. D. Liu, Q. M. Wang, *Nat. Commun.* **2019**, *10*, 4032.

[13] Z.-R. Yuan, Z. Wang, B.-L. Han, C.-K. Zhang, S. S. Zhang, Z.-Y. Zhu, J.-H. Yu, T.-D. Li, Y.-Z. Li, C.-H. Tung, D. Sun, *Angew. Chem., Int. Ed.* **2022**, *61*, e202211628.

[14] a) S. Sharma, K. K. Chakrahari, J. Y. Saillard, C. W. Liu, *Acc. Chem. Res.* **2018**, *51*, 2475. b) T. A. D. Nguyen, Z. R. Jones, B. R. Goldsmith, W. R. Buratto, G. Wu, S. L. Scott, T. W. Hayton, *J. Am. Chem. Soc.* **2015**, *137*, 13319. c) C. Sun, N. Mammen, S. Kaappa, P. Yuan, G. Deng, C. Zhao, J. Yan, S. Malola, K. Honkala, H. Häkkinen, B. K. Teo, N. Zheng, *ACS Nano* **2019**, *13*, 5975. d) A. W. Cook, Z. R. Jones, G. Wu, S. L. Scott, T. W. Hayton, *J. Am. Chem. Soc.* **2018**, *140*, 394. e) A. Baghdasaryan, C. Besnard, L. M. Lawson Daku, T. Delgado, T. Burgi, *Inorg. Chem.* **2020**, *59*, 2200. f) A. Ghosh, R. W. Huang, B. Alamer, E. Abou-Hamad, M. N. Hedhili, O. F. Mohammed, O. M. Bakr, *ACS Mater. Lett.* **2019**, *1*, 297. g) J. Li, H. Z. Ma, G. E. Reid, A. J. Edwards, Y. Hong, J. M. White, R. J. Mulder, R. A. J. O'Hair, *Chem. - Eur. J.* **2018**, *24*, 2070. h) M. Qu, F.-Q. Zhang, D.-H. Wang, H. Li, J.-J. Hou, X.-M Zhang, *Angew. Chem., Int. Ed.* **2020**, *59*, 6507. i) C. Dutta, S. Maniappana, J. Kumar, *Chem. Sci.* **2023**, *14*, 5593. j) R. Czerwieniec, M. J. Leitl, H. H. H. Homeier, H. Yersin, *Coord. Chem. Rev.* **2016**, *325*, 2. k) D. Felder, J.-F. Nierengarten, F. Barigelletti, B. Ventura, N. Armaroli, *J. Am. Chem. Soc.* **2001**, *123*, 6291.

[15] a) V. Lavallo, Y. Canac, C. Prasang, B. Donnadieu, G. Bertrand, *Angew. Chem., Int. Ed.* **2005**, *44*, 5705. b) F. Dahcheh, D. Martin, D. W. Stephan, G. Bertrand, *Angew. Chem., Int. Ed.* **2014**, *53*, 13159. c) E. Welz, I. Krummenacher, B. Engels, H. Braunschweig, *Science* **2018**, *359*, 892. d) M. A. Légaré, M. Rang, G. Bélanger-Chabot, J. I. Schweizer, I. Krummenacher, R. Bertermann, M. Arrowsmith, M. C. Holthausen, H. Braunschweig, *Science* **2019**, *363*, 1329. e) M. A. Légaré, G. Belanger-Chabot, M. Rang, R. D. Dewhurst, I. Krummenacher, R. Bertermann, H. Braunschweig, *Nat. Chem.* **2020**, *12*, 1076.

[16] a) D. Di, A. S. Romanov, L. Yang, J. M. Richter, J. P. H. Rivett, S. Jones, T. H. Thomas, M. A. Jalebi, R. H. Friend, M. Bochmann, D. Credgington, *Science* **2017**, *356*, 159. b) R. Hamze, J. L. Peltier, D. Sylvinson, M. Jung, J. Cardenas, R. Haiges, M. Soleilhavoup, R. Jazzar, P. I. Djurovich, G. Bertrand, M. E. Thompson, *Science* **2019**, *363*, 601. c) P. J. Conaghan, C. S. B. Matthews, F. Chotard, S. T. E. Jones, N. C. Greenham, M. Bochmann, D. Credgington, A. S. Romanov, *Nat. Commun.* **2020**, *11*, 1758. d) R. Hamze, S. Shi, S. C. Kapper, D. S. Muthiah Ravinson, L. Estergreen, M. C. Jung, A. C. Tadle, R. Haiges, P. I. Djurovich, J. L. Peltier, R. Jazzar, *J. Am. Chem. Soc.* **2019**, *141*, 8616. e) P. J. Conaghan, S. M. Menke, A. S. Romanov,

[17] E. Nag, S. Battuluri, K. C. Mondal, S. Roy, *Chem. - Eur. J.* **2022**, *28*, e202202324.

[18] a) M. Peters, A. Doddi, T. Bannenberg, M. Freytag, P. G. Jones, M. Tamm, *Inorg. Chem.* **2017**, *56*, 10785. b) A. Doddi, D. Bockfeld, T. Bannenberg, P. G. Jones, M. Tamm, *Angew. Chem., Int. Ed.* **2014**, *53*, 13568; c) A. Doddi, D. Bockfeld, T. Bannenberg, P. G. Jones, M. Tamm, *Angew. Chem.* **2014**, *126*, 13786.

[19] a) A. Doddi, D. Bockfeld, A. Nasr, T. Bannenberg, P. G. Jones, M. Tamm, *Chem. - Eur. J.* **2015**, *21*, 16178. b) A. Doddi, M. Peters, M. Tamm, *Chem. Rev.* **2019**, *119*, 6994.

[20] V. A. K. Adiraju, M. Yousufuddin, H. V. Rasika Dias, *Dalton Trans.* **2015**, *44*, 4449.

[21] A. Kulkarni, S. Arumugam, M. Francis, P. G. Reddy, E. Nag, S. M. N. V. T. Gorantla, K. C. Mondal, S. Roy, *Chem. - Eur. J.* **2021**, *27*, 200.

[22] S. Roy, K. C. Mondal, S. Kundu, B. Li, C. J. Schürmann, S. Dutta, D. Koley, R. Herbst-Irmer, D. Stalke, H. W. Roesky, *Chem. - Eur. J.* **2017**, *23*, 12153.

[23] O. Back, B. Donnadieu, P. Parameswaran, G. Frenking, G. Bertrand, *Nat. Chem.* **2010**, *2*, 369.

[24] E. Nag, S. Battuluri, B. B. Sinu, S. Roy, *Inorg. Chem.* **2022**, *61*, 13007.

[25] a) S. Gambarotta, G. Floriani, A. Chiesi-Villa, C. J. Guastini, *Chem. Soc. Chem. Commun.* **1983**, 1156. b) M. Stollenz, F. Meyer, *Organometallics* **2012**, *31*, 7708.

[26] E. Kounalis, M. Lutz, D. L. J. Broere, *Organometallics* **2020**, *39*, 585.

[27] M. Schütz, C. Gemel, M. Muhr, C. Jandl, S. Kahlal, J.-Y. Saillard, R. A. Fischer, *Chem. Sci.* **2021**, *12*, 6588.

[28] V. W.-W. Yam, K.-K. Lee, K. K. Cheung, H.-K. Lee, W.-P. Leung, *J. Chem. Soc. Dalton Trans.* **1996**, 2889.

[29] a) W.-H. Chan, Z.-Z. Zhang, T. C. W. Mak, C.-M. Che, *J. Organomet. Chem.* **1998**, *556*, 169. b) Y.-G. Ma, W.-H. Chan, X.-M. Zhou, C.-M. Che, *New J. Chem.* **1999**, *23*, 263.

[30] a) A. Sundararaman, L. N. Zakharov, A. L. Rheingold, F. Jäkle, *Chem. Commun.* **2005**, 1708. b) F. Jäkle, *Dalton Trans.* **2007**, 2851.

[31] A. M. James, R. K. Laxman, F. R. Fronczek, A. W. Maverick, *Inorg. Chem.* **1998**, *37*, 3785.

[32] a) H. V. R. Dias, H. V. K. Diyabalanage, M. A. Rawashdeh-Omary, M. A. Franzman, M. A. Omary, *J. Am. Chem. Soc.* **2003**, *125*, 12072. b) M. A. Omary, M. A., Rawashdeh-Omary, M. W. A. Gonser, O. Elbjeirami, T. Grimes, T. R. Cundari, H. V. K. Diyabalanage, C. S. P. Gamage, H. V. R. Dias, *Inorg. Chem.* **2005**, *44*, 8200. c) H. V. R. Dias, H. V. K. Diyabalanage, M. G. Eldabaja, O. Elbjeirami, M. A. Rawashdeh-Omary, M. A. Omary, *J. Am. Chem. Soc.* **2005**, *127*, 7489.

[33] a) X. S. Han, X. Q. Luan, H. F. Su, J. J. Li, S. F. Yuan, Z. Lei, Y. Pei, Q. M. Wang, *Angew. Chem., Int. Ed.* **2020**, *59*, 2309; b) X. S. Han, X. Q. Luan, H. F. Su, J. J. Li, S. F. Yuan, Z. Lei, Y. Pei, Q. M. Wang, *Angew. Chem.* **2020**, *132*, 2329. c) L. L. M. Zhang, G. Zhou, G. Zhou, H. K. Lee, N. Zhao, O. V. Prezhdo, T. C. Mak, *Chem. Sci.* **2019**, *10*, 10122. d) H. T. Lin, K. B. Cai, H. Y. Huang, T. N. Lin, J. L. Shen, C. A. J. Lin, C. T. Yuan, *J. Lumin.* **2017**, *187*, 269.

[34] L. Zhang, K. W. Cheah, *Sci. Rep.* **2018**, *8*, 8832.

[35] K. Xu, B. L. Chen, R. Zhang, L. Liu, X. X. Zhong, L. Wang, F. Y. Li, G. H. K. Li, A. Alamry, F. B. W. Y. Wong, H. M. Qin, *Dalton Trans.* **2020**, *49*, 5859.

[36] Y. Hou, Y. Wang, T. Xu, Z. Wang, W. Tian, D. Sun, X. Yu, P. Xing, J. Shen, X. Xin, J. Hao, *Chem. Mater.* **2022**, *34*, 8013.

[37] M. Xie, C. Han, J. Zhang, G. Xie, H. Xu, *Chem. Mater.* **2017**, *29*, 6606.

[38] a) J. R. Kirchhoff, R. E. Gamache Jr., M. W. Blaskie, A. A. Del Paggio, R. K. Lengel, D. R. Mcmillin, *Inorg. Chem.* **1983**, *22*, 2380. b) T. P. Yoon, M. A. Ischay, J. Du, *Nat. Chem.* **2010**, *2*, 527. c) D. M. Schultz, T. P. Yoon, *Science* **2014**, *343*, 1239176. d) J. M. R. Narayanam,

J. W. Tucker, C. R. J. Stephenson, *J. Am. Chem. Soc.* **2009**, *131*, 8756.

[39] E. Nag, S. M. N. V. T. Gorantla, S. Arumugam, A. Kulkarni, K. C. Mondal, S. Roy, *Org. Lett.* **2020**, *16*, 6313.

[40] *Bruker APEX4, SAINT and SADABS*, Bruker AXS Inc, Madison, Wisconsin, USA **2021**.

[41] L. Krause, R. Herbst-Irmer, G. M. Sheldrick, D. Stalke, *J. Appl. Cryst.* **2015**, *48*, 3.

[42] G. M. Sheldrick, *Acta Cryst. Section A* **2015**, *71*, 3.

[43] C. B. Hübschle, G. M. Sheldrick, B. Dittrich, *J. Appl. Cryst.* **2011**, *44*, 1281.